2020-03

Distortional buckling of perforated cold-formed steel beams subject to uniformly distributed transverse loads

Voudouris, Vlasios

10.1016/j.tws.2019.106569
Thin-Walled Structures
Elsevier BV

Published in
Thin-Walled Structures, Vol. 148, March 2020
https://doi.org/10.1016/j.tws.2019.106569
Accepted 10 December 2019

Distortional buckling of perforated cold-formed steel beams subject to uniformly distributed transverse loads

Nan-ting Yu[a,b], Boksun Kim[b], Long-yuan Li[b], Wei-jian Hong[a] and Wei-bin Yuan[a*]

(a) College of Architecture and Civil Engineering, Zhejiang University of Technology, Hangzhou 310023, PR China

(b) School of Engineering, Computing and Mathematics, University of Plymouth, Plymouth PL4 8AA, UK

Abstract: Thin-walled channel beams are easily punched with circular holes on the web to allow the access for services such as plumbing pipes and electric wires. The presence of the holes can alter the stress distribution in the member and reduce the cross-sectional property. Consequently, it changes its buckling mode. Since perforated cold-formed steel beams are usually placed between main structural frame and corrugated roof, the most common loading case is the uniformly distributed transverse load. Recent work by Chen and Li has given the solution for distortional buckling of channel-, zed- and sigma- sections subject to the uniformly distributed transverse load. This paper is an extension of Chen and Li's research to explore the distortional buckling behaviour of perforated cold-formed steel beams with holes. The effect of perforations on the critical stress is evaluated. A new model is deduced to predict the critical stress of distortional buckling by reducing the stiffness of the vertical spring. The Rayleigh-Ritz method is used to solve eigenvalue problems. In order to validate the analytical model, finite element analyses have been performed by using ANSYS. When the beam is longer than 3500 mm, the critical stress computed from the analytical model matches well with the critical stress acquired from the finite element analyses.

Keywords: Distortional buckling; cold-formed steel; perforations; finite element analysis; stress gradient.

1. Introduction

Cold-formed steel (CFS) members are considered as the important load carrying members in building industries due to their unique material properties. The yield strength of CFS can be as high as 550 MPa and its thickness can be less than 2 mm. Unlike hot-rolled steel sections, a CFS section has low lateral and torsional stiffness due to its thin and open geometry. For this reason, it is susceptible for CFS sections to buckle. To release the space of a structure, perforated cold-formed steel (PCFS) beams tend to be used as secondary load carrying members in buildings to let the plumbing pipes and electric wires pass through. However, the restraint of the web to the compressed flange is reduced owing to the perforation patterns in the web. This leads to PCFS beams being sensitive to distortional buckling.

Lau and Hancock [1-2] firstly presented the concept of distortional buckling, which can be described as the buckling of compressed flange-lip component with respect to the web-flange

junction, meanwhile the web undergoes bending . In Lau and Hancock's model, the flange-lip system can be isolated and considered alone, the influence of the web on the compressed flange and lip was represented by the rotational and lateral spring. Since then, great efforts have been made on developing analytical models to determine the critical stress of distortional buckling of CFS members. Teng et al. [3] extended Lau and Hancock's approach for the CFS sections subject to combined axial compression and biaxial bending. In Eurocode 3, the stiffener was assumed to be supported at the elastic foundation with continuous spring along the length [4]. Later, Li and Chen [5] considered the bending behaviour of the stiffener by using the vertical spring to replace the rotational spring. More recently, Zhu et al. [6-8] utilised a plate model with an angle stiffener to replace the flange-lip system, the energy method was used to obtain the critical stress. In addition, the numerical methods such as finite strip method (FSM), finite element analysis (FEA) and generalised beam theory (GBT) [9] have also been regarded as the suitable approaches to calculate the distortional buckling stress of CFS members.

Similar to CFS sections, the PCFS members may suffer three types of buckling, such as local buckling, distortional buckling and lateral-torsional buckling. However, the presence of the holes will not only alter the stress distribution in the member but also reduce the cross-sectional property, and consequently change the buckling modes. The reductions of the critical buckling stress and ultimate strength are mainly depending on the shape, arrangement and size of the holes. Miller and Peköz [10] assumed that the web was idealised as two unstiffened element and modify the unified effective width method for the perforated studs. Moen and Schafer [11] presented simplified expressions for critical elastic buckling stress of perforated thin plates, for both stiffened and unstiffened elements. Subsequently, they proposed analytical approaches for calculating the global, distortional and local buckling stress of CFS members with holes [12]. Yu et al. [13-14] modified the EN 1993-1-3 model and Lau and Hancock's model to determine the critical distortional buckling stress of PCFS beams subject to pure bending. They found that the critical stress obtained from the modified Hancock's model is more accurate.

FSM was regarded as an effective approach for predicting the elastic buckling stress of PCFS members by some researchers. For instance, Tovar and Sputo [15-16] presented some perforated web models to represent the influence of the holes by using FSM. Smith and Moen [17] introduced the approximate FSM for elastic buckling analysis of PCFS columns, in which the principle of reduced thickness was considered. Pham [18] provided the solutions to find out the shear buckling loads of perforated thin plates and PCFS sections using spline FSM.

For the elastic buckling controlled failure, the direct strength method (DSM) can predict the ultimate strength of the CFS members accurately [19]. It is worth noting that some experimental work has been conducted to extend the existing DSM for PCFS members. Moen and Schafer [20] observed the relation between buckling behaviour and tested load-displacement response of PCFS columns with slotted holes. Zhao et al. [21] presented experimental investigations on PCFS beams with square holes subject to four-point bending, from which the modified DSM formulas were proposed. Wang and Young [22-23] preformed the beam tests of built-up PCFS sections, from which the relative extended DSM was carried out.

PCFS beams are usually placed between the main structure and roof as the secondary load carrying members. Thus, the most common loading case of the PCFS members is the uniformly distributed transverse load rather than pure bending. If the member is subject to the uniformly

distributed transverse load, the stress distribution along the longitudinal direction will be different. Most existing analytical approaches were developed for the beams with pure bending or pure compression, which cannot be applied to the beams with stress gradient. Little information about the buckling behaviour of PCFS sections under the uniformly distributed transverse load can be discovered in the literature. Li [24] investigated the lateral-torsional buckling behaviour of CFS zed-purlins under both down and uplift load and presented an analytical model to predict the critical load. Chu et al. [25-26] utilised the semi-analytical FSM to study the local and distortional buckling of CFS zed- and channel-sections under the uniformly distributed transverse load, from which the influence of stress gradient on the buckling behaviour of the members was highlighted. Chen and Li [27] evaluated the effect of stress gradient on the distortional buckling of CFS beams. However, the sections they investigated are plain sections with no holes.

This paper aims to develop a solution for the distortional buckling stress of PCFS beams under a uniformly distributed transverse load. The analytical model for computing the distortional critical stress is derived which is based on Chen and Li's work [27]. The effect of holes on the critical stress of distortional buckling is reckoned. The Rayleigh-Ritz method is used to solve the eigenvalue problem. In order to validate the analytical results, FEA is performed by using commercial software ANSYS. Comparisons between the theoretical result and the FEA data are presented in this paper.

2. Analytical model

The cross section of a PCFS beam is shown in Fig.1a, which is the same as that in the literature [13] and [14]. The notations of the web height, flange width, lip length and section thickness are defined as h, b, c and t, respectively. The circular holes are punched in the centreline of the web evenly, with a diameter defined as d. The shaded part represents the solid area in the perforated strip. To simplify the calculation, the opening area is assumed to be same as the solid area in the perforated strip of the plate. Therefore, the length of the beam is expressed as $n_h \pi d/2$, where n_h is a random constant, representing the total number of the holes, as shown in Fig.1b.

Fig.2 shows Li and Chen's method [5], the difference with the model developed by Lau and Hancock [1] is that the vertical spring at the centroid of the compressed flange-lip component is used to replace the rotational spring at the flange-web corner. It is very similar to the one used in Eurocode 3 [4], which represents the restraint of web to the compressed flange-lip component, however it considers the flexural behaviour of the flange-lip component itself. To apply the Li and Chen's model for PCFS beams, the stiffness of the vertical spring should be reduced to take account the influence of the web openings.

It is clear that the spring stiffness can be determined by means of the flexural stiffness of the web and flange of the section. The unit load F at the centroid of the compressed flange and lip is used to determine the modified stiffness of the vertical spring, see Fig. 3. Then, the strain energy of the compressed flange and web due to bending can be determined by the following formula,

$$U=\frac{1}{2EI_1}\int_0^{b-y_0}(Fy)^2dy+\frac{1}{2EI_1}\int_0^{h}[F(b-y_0)-\frac{F(b-y_0)}{h}z]^2dz$$
$$+(\frac{1}{2EI_2}-\frac{1}{2EI_1})\int_{\frac{h-d}{2}}^{\frac{h+d}{2}}[F(b-y_0)-\frac{F(b-y_0)}{h}z]^2dz \quad (1)$$

where y_0 is the horizontal distance between the shear centre and centroid, E is the Young's modulus, I_1 and I_2 are the moment of inertia of the area with and without holes, respectively.

The deflection of the vertical spring is

$$\delta=\frac{\partial U}{\partial F}$$
$$=\frac{F(b-y_0)^3}{3EI_1}+\frac{F(b-y_0)^2h}{3EI_1}+(\frac{1}{EI_2}-\frac{1}{EI_1})F(b-y_0)^2\frac{h}{3}[(\frac{h+d}{2h})^3-(\frac{h-d}{2h})^3] \quad (2)$$

The modified stiffness of the vertical spring can be obtained according to Eq. (1) and Eq. (2), which is given as,

$$k'_z=\frac{F}{\delta}=\frac{3D}{(b-y_0)^2(b-y_0+h)}\times\frac{1}{1+\frac{1}{4}(\frac{d}{h})\left[\frac{3+(d/h)^2}{1+(b-y_0)/h}\right](\frac{D}{D_d}-1)} \quad (3)$$

where D is the flexural rigidity of the stiffened element and the web strip without holes, D_d is the flexural rigidity of the web strip with holes. In this case, D_d =0.5D due to the concept of equal width. If there are no holes in the web (d = 0), Eq. (3) could be expressed as follows,

$$k_{z0}=\frac{1}{\frac{(b-y_0)^3}{3D}+\frac{(b-y_0)^2}{\frac{3D}{h}}} \quad (4)$$

where 3D/h represents the unmodified rotational spring stiffness at the web-flange corner.

It should be pointed out herein that the stiffness of rotational stiffness in Hancock's model [2] is modified and multiplying the reduction factor which is obtained as follows,

$$k_\phi=\frac{2Et^3}{5.46[h+\frac{4}{3}(b-y_0)]}(1-1.11\frac{\sigma_{od}}{Et^2}\frac{h^4\lambda_{cr}^2}{12.56\lambda_{cr}^4+2.192h^4+13.39\lambda_{cr}^2h^2}\frac{h}{h-2z_0}) \quad (5)$$

where λ_{cr} is the half-wavelength and σ_{od} is the compressive stress of the web. Eq. (5) can be solved by the iterative procedure which could be found in Literature [14]. In the following calculation, Eq. (5) is used to replace 3D/h in Eq. (4).

Let

$$\alpha=\frac{1}{1+\frac{1}{4}(\frac{d}{h})\left[\frac{3+(d/h)^2}{1+(b-y_0)/h}\right](\frac{D}{D_d}-1)} \quad (6)$$

The vertical spring stiffness of modified Li and Chen's model for PCFS beams is

$$k_z = \alpha \cdot \frac{1}{\frac{(b-y_0)^3}{3D} + \frac{(b-y_0)^2}{k_\phi}} \tag{7}$$

Fig. 4 shows that the moment curve is parabolic when the beam is subject to uniformly distributed transverse loads and the moment curve is straight when the beam is subject to pure bending. For this reason, the wave lengths of the distortional buckling mode under pure bending are equal, but the wave lengths of the distortional buckling mode under uniformly distributed transverse loads are unequal due to the moment gradient effect. Hence, the buckling modes of the PCFS beam not only depend on the cross-section dimension but also the length of the beam, as well as the perforations. For simplicity, the uniformly distributed transverse load is supposed to be applied at the shear centre so that the member will not twist.

If the PCFS beam is simply supported and subject to a uniformly distributed transverse load, the internal bending moment can be described as follows,

$$M(x) = \frac{q_z l}{2} x - \frac{1}{2} q_z x^2 \tag{8}$$

Hence, the external force in the flange-lip component is

$$P = \sigma_x A = \frac{M(x)}{M_{cr}} \sigma_{cr} A = \frac{4x(l-x)}{l^2} \sigma_{cr} A \tag{9}$$

However, when the simply supported beam is subject to the pure bending, the relative external force in the flange-lip component is

$$P = \sigma_{cr0} A \tag{10}$$

where q_z is the uniformly distributed transverse load, $M_{cr} = q_z l^2/8$ is the largest internal moment, σ_{cr} is corresponding critical stress when it is subject to uniformly distributed transverse loads, $A=(b+c)t$ is the cross-section area of the compressed flange and lip component, σ_{cr0} is critical stress when it is subject to pure bending.

When the beam occurs a distortional buckling, the buckled flange-lip system will have translational and rotational displacements. The strain energy due to the buckling displacements stored in the flange-lip system and the loss of potential energy can be evaluated. According to Chen and Li's model [27], they can be defined as follows,

$$U_0 = \frac{1}{2} \int_0^l [(EI_w + EI_y b^2)(\frac{d^2\phi}{dx^2})^2 + GJ(\frac{d\phi}{dx})^2 + k_z (b-y_0)^2 \phi^2] dx \tag{11}$$

$$W_p = \frac{z_0^2 + (b-y_0)^2 + r_c^2}{2} \int_0^l P(\frac{d\phi}{dx})^2 dx \tag{12}$$

where l is length of the beam, I_w is the warping constant which is equal to zero in present study, I_y is the second moment of the section area about the y axis, Φ is the rotation of the section about the shear centre, G is the shear modulus, J is the St. Venant torsional constant, k_z is the

stiffness of the vertical spring, z_0 is the vertical distance between the centroid and the shear centre and r_c is the polar radius of gyration of the cross section about the centroid. Some of the above parameters can be obtained as follows,

$$\phi(x) = a_1 \sin\frac{\pi x}{l} + a_2 \sin\frac{2\pi x}{l} + a_3 \sin\frac{3\pi x}{l} + \cdots + a_n \sin\frac{n\pi x}{l} \tag{13}$$

$$y_0 = b - \frac{b^2/2 + bc}{b + c} \tag{14}$$

$$z_0 = \frac{c^2/2}{b + c} \tag{15}$$

$$I_y = \frac{1}{12}bt^3 + btz_0{}^2 + \frac{1}{12}c^3t + ct(\frac{c}{2} - z_0)^2 \tag{16}$$

$$I_z = \frac{1}{12}tb^3 + bt(y_0 - \frac{b}{2})^2 + \frac{1}{12}ct^3 + cty_0{}^2 \tag{17}$$

$$G = \frac{E}{2(1+\mu)} \tag{18}$$

$$J = \frac{(b+c)t^3}{3} \tag{19}$$

$$r_c{}^2 = \frac{1}{A}(I_y + I_z) \tag{20}$$

where μ is the Poisson's ratio, a_1, a_2, … , a_n are arbitrary constants, n is not equal to m and the sum $(m+n)$ is even.

The critical stress of torsional and flexural-torsional buckling of the flange-lip system with spring support can be determined by using energy method, that is,

$$\partial^2\Pi = \partial^2(U_0 - W_p) = 0 \tag{21}$$

Substituting Eq. (9), Eq. (11) and Eq. (12) into Eq. (21) yields,

$$\frac{z_0^2 + (b-y_0)^2 + r_c^2}{l^2}[\sum_{n=1}^{\infty}(\frac{n^2\pi^2}{3} - 1)a_n^2 - 4\sum_n\sum_m(\frac{mn}{(m+n)^2} + \frac{mn}{(n-m)^2})a_m a_n]2\sigma_{cr} - \sum_{n=1}^{\infty}[\frac{EI_w + EI_y b^2}{A}\frac{n^4\pi^4}{l^4} + \frac{GJ}{A}\frac{n^2\pi^2}{l^2} + \frac{k_z(b-y_0)^2}{A}]a_n^2 = 0 \tag{22}$$

Eq. (22) can be used to predict the critical stress of distortional buckling of CFS beams without holes subject to uniform distributed transverse loads. However, to determine the critical stress of distortional buckling of PCFS beams, the stiffness of the vertical spring k_z must be modified. Therefore, Eq. (7) should be applied into Eq. (22). Based on the Rayleigh-Ritz method, deriving with respect to a_1, a_2, … , a_n is equal to zero. The following type of linear equations in a_1, a_2, … , a_n can be acquired.

$$\left\| \begin{bmatrix} a_{11} & \cdots & a_{1n} \\ \vdots & \ddots & \vdots \\ a_{n1} & \cdots & a_{nn} \end{bmatrix} - \sigma_{cr} \begin{bmatrix} b_{11} & \cdots & b_{1n} \\ \vdots & \ddots & \vdots \\ b_{n1} & \cdots & b_{nn} \end{bmatrix} \right\| = 0 \tag{23}$$

in which,

$$a_{ij} = 0 \qquad (i \neq j) \tag{24a}$$

$$a_{nn} = \frac{(EI_w + EI_y b^2)(\frac{n\pi}{l})^4 + GJ(\frac{n\pi}{l})^2 + k_z(b - y_0)^2}{A} \tag{24b}$$

$$b_{pn} = 0 \qquad (p \neq n; p + n = odd) \tag{24c}$$

$$b_{mn} = \frac{z_0^{\,2} + (b - y_0)^2 + r_c^2}{l^2}[-16 \times \frac{nm(n^2 + m^2)}{(n^2 - m^2)^2}] \tag{24d}$$

$$b_{nn} = \frac{z_0^{\,2} + (b - y_0)^2 + r_c^2}{l^2}[2 \times (\frac{n^2\pi^2}{3} - 1)] \tag{24e}$$

Eq. (23) is a matrix with infinite dimensions which represents an eigenvalue problem, the eigenvalues are computed by software MATLAB. Among all the eigenvalues, the smallest one is the critical stress of distortional buckling. It is well known that the half-wave length of distortional buckling of the CFS beam is about 500 mm although the exact length depends on the section dimensions. Table 1 shows the exact distortional half-wave lengths obtained using the free software package CUFSM [28] for the CFS channel-sections produced by Albion Section. Therefore the largest value of *n* can be evaluated by the beam length, e.g. for the 3000 mm beam if its half-wave length is 500 mm, *n* should be at least taken as 6.

When the beams are subject to pure bending, Substituting Eq. (10), Eq. (11) and Eq. (12) into Eq. (21) yields,

$$\sigma_{cr0} = \frac{(EI_w + EI_y b^2)(\frac{n\pi}{l})^2 + GJ + k_z(b - y_0)^2(\frac{l}{n\pi})^2}{A(z_0^{\,2} + (b - y_0)^2 + r_c^2)} \tag{25}$$

It should be mentioned that the rotational stiffness of spring also needs to be modified to calculate the critical stress of distortional buckling of PCFS beams which had been derived in Ref. [13].

Fig.5 shows the critical stresses of the distortional buckling of PCFS beams under uniformly distributed transverse loads and pure bending, which are calculated from Eq. (23) and Eq. (25). It can be observed that the critical stress curve for uniformly distributed transverse loads is highly depending on the beam length. It decreases dramatically with the increase of the length when the beam length is less than 3000 mm. The decrease diminishes when the beam length is longer than 4500 mm. The dash line is for the case subject to pure bending which is obtained from Eq. (25). As shown in Fig. 5, the critical stress of uniformly distributed transverse loads is continually higher than that of pure bending and when the beam is long enough these two

critical stresses tend to be the close. In most practical cases, these differences should be taken into account.

3. Finite Element Analysis and Validation

In order to verify the proposed analytical approach, finite element analysis was performed by using a commercial software program ANSYS. The cross-sectional dimension of the beam was the same as C20625 (h=200 mm, b=65 mm, c= 20 mm and t=2.5 mm) which was chosen from Albion sections. Various lengths and hole sizes of the PCFS beam were analysed in which the PCFS beams were modelled by using four-node shell 181. The fine element sizes were controlled not to exceed 10 mm, Fig.6 shows a typical element mesh used in the analysis. The material properties of the beam analysed are assumed to have Young's modulus of 205 GPa and Poisson's ratio of 0.3.

The boundary conditions were considered to have zero lateral and transverse displacements (UX=UY=0) and zero rotation about the longitudinal axis (ROTZ=0) for the web, flange and lip lines at the two ends. To avoid the rigid movement, one node located in the middle of the web at one end was set as zero longitudinal displacement (UZ=0). It should be noted that when the length of the beam increases, the distortional buckling mode will be gradually coupled with lateral-torsional mode, and hence the relevant critical stress will reduce. In this present study, only the distortional buckling mode was examined. Hence, the two corner line between the web and flange were both restrained laterally (UX=0) to prevent the lateral-torsional buckling occurred.

The uniformly distributed transverse load q_z was assumed to be applied at the shear centre of the beam, so that it can undergo bending without twist. There are two ways to simulate this situation. One is to apply the distributed transverse load on the plate which has infinite rigidity. The length of the plate is equal to the beam length and its width is same as the distance between the web line and the shear centre, as shown in Fig.7 (a). The other way is to apply distributed transverse loads at the web directly combined with an equivalent distributed twist moment. The value of the twist moment is equal to the value of transverse load times the distance between the web and the shear centre (see Fig.7 (b)). For simplicity, the second loading condition (Fig.7 (b)) was utilised in this FEA.

Fig.8 shows the typical distortional buckling modes of PCFS beams with different hole sizes under a uniformly distributed transverse load. As can be seen in the Fig.8, the CFS channel beams with and without holes have the analogous distortional buckling modes which were controlled by the rotation of the compressive flange-lip component with respect to the web-flange corner. Moreover, it is interesting to observe that the half-wave lengths were different along the beam length. This is because when the beam is subject to uniformly distributed transverse load, the longitudinal stresses vary parabolically along the beam length. The highest compressive stress appears in the central region, which leads to the shortest half-wave length; whereas the half-wave lengths near the two beam ends are the largest because the stresses are the lowest there. The varied compressive stresses produce the distortional buckling modes with several buckling waves, each has different half-wave lengths.

To validate the proposed analytical approach, Fig.9 compares the critical stress of PCFS beams with different hole sizes obtained from Eq. (23) and those obtained from FEA, where σ_{cr} is the critical stress and σ_y is the yield stress (σ_y = 450MPa, obtained from Albion sections). It can be

observed from the comparison that the tendency of the critical stress curves was similar. As the size of holes increased, the relative critical stress of the beam decreased. It is mainly because the restraint of the compressed flange and lip from the web is weaker for the PCFS beam with larger holes.

The results given in Fig.9 shows that when the beam length is longer than 3500 mm, the present analytical solution matches very well with the data obtained from FEA. However, for the short beams, the results calculated from Eq. (23) are much higher than that obtained from FEA, as detailed in the red box in Fig.9. This is because when the beams are subject to the uniformly distributed transverse load, the shear stress near the support in the short beam is much severer than corresponding bending stress. Consequently, short PCFS beams may buckle due to the shear stress rather than the bending stress. In addition, stress concentration exists near the web opening which may induce a local buckling. All of these buckling modes are included in the FEA but not in the present analytical solution. This is why the present critical stress is higher than that FEA predicted ones for short beams. Nevertheless, with the increase of the beam length, the present solution becomes very close to the FEA predicted results.

It should be mentioned that, the stress gradient affects not only the distortional buckling behavior but also the behavior of other buckling types of PCFS beams, such as the shear buckling and the lateral-torsional buckling. This is generally owing to the variation of pre-buckling stresses along the longitudinal direction. However, the effect mechanisms of the stress gradient on different types of buckling may be also different. In the present paper, only distortional buckling of PCFS beams has been investigated. The other buckling types of PCFS will be investigated as our future work.

4. Conclusions

This paper has presented an analytical and numerical study on the distortional buckling behaviour of the PCFS beams subject to uniformly distributed transverse loads. The equations for predicting the distortional buckling stress of PCFS beams have been derived using the energy method. The model has been compared against the results obtained from the FEA. From the analytical and numerical results obtained in this research, the conclusions can be made as follows:

- The distortional buckling stress of PCFS beams decreases with the increase of the diameter of the perforation. The influence of circular holes can be evaluated by reducing the vertical spring stiffness of the compressed flange-lip component adopted in the buckling model.
- The critical stress of distortional buckling of a PCFS beam subject to uniformly distributed transverse load is larger than the same beam subject to pure bending. However, the difference between their two critical stresses decreases with the increase of their beam lengths.
- The effect of stress gradient on the distortional buckling is highly depending on the length of the beam, it reduces with the length increases.
- The half-wave lengths of the distortional buckling mode of the PCFS beams are different along the beam length when it is subject to uniformly distributed transverse loads and the largest deflection occurred at the mid-span.

Acknowledgement

The first author would like to acknowledge the financial support received from the Chinese Scholarship Council and the studentship received from the University of Plymouth for his PhD study in the United Kingdom. The corresponding author would like to acknowledge the financial supports by the Natural Science Foundation of Zhejiang Province (No. LY19E080020).

References

[1] Lau S. C. W. and Hancock G. J. (1987): Distortional buckling formulas for channel columns. Journal of Structural Engineering, 113(5), 1063-1078.

[2] Hancock G. J. (1997): Design for distortional buckling of flexural members. Thin-Walled Structures, 27(1), 3-12.

[3] Teng J. G., Yao J. and Zhao Y. (2003): Distortional buckling of channel beam-columns. Thin-Walled Structures, 41(7), 595-617.

[4] EN1993-1-3 (2006): Design of Steel Structures. Part 1-3: General rules- Supplementary rules for cold-formed members and sheeting. BSI, Brussels.

[5] Li L. Y. and Chen J. K. (2008): An analytical model for analysing distortional buckling of cold-formed steel sections. Thin-walled Structures, 46(12), 1430-1436.

[6] Zhu J. and Li L. Y. (2016): A stiffened plate buckling model for calculating critical stress of distortional buckling of CFS beams. International Journal of Mechanical Sciences, 115-116, 457-464.

[7] Huang X. H. and Zhu J. (2016): A stiffened-plate buckling model for calculating critical stress of distortional buckling of CFS columns. International Journal of Mechanical Sciences, 119, 237-242.

[8] Huang X. H., Yang J., Liu Q. F., Zhu J., Li B., Wang F. L. (2018): A simplified flange-lip model for distortional buckling of cold-formed steel channel-sections with stiffened web. International Journal of Mechanical Sciences,136, 451-459.

[9] Jiang C. and Davies J.M. (1997): Design of thin-walled purlins for distortional buckling. Thin-Walled Structures, 29(1-4), 189-202.

[10] Miller T. H. and Peköz T. (1994): Unstiffened strip approach for perforated wall studs. Journal of Structural Engineering, 120(2), 410-421.

[11] Moen C. D. and Schafer B. W. (2009): Elastic buckling of thin plates with holes in compression or bending. Thin-Walled Structures, 47(12), 1597-1607.

[12] Moen C. D. and Schafer B. W. (2009): Elastic buckling of cold-formed steel columns and beams with holes. Engineering Structures, 31(12), 2812-2824.

[13] Yuan W. B., Yu N. T. and Li L. Y. (2017): Distortional buckling of perforated cold-formed steel channel-section beams with circular holes in web. International Journal of Mechanical Sciences, 126, 255-260.

[14] Yu N. T., Kim B., Yuan W. B., Li L. Y. and Yu F. (2019): An analytical solution of distortional buckling resistance of cold-formed steel channel-section beams with web openings. Thin-Walled Structures, 135, 446-452.

[15] Sputo T. and Tovar J. (2005): Application of direct strength method to axially loaded perforated cold-formed steel studs: Longwave buckling. Thin-Walled Structures, 43(12), 1852-1881.

[16] Tovar J. and Sputo T. (2005): Application of direct strength method to axially loaded perforated cold-formed steel studs: Distortional and local buckling. Thin-Walled Structures, 43(12), 1882-1912.

[17] Smith F. H. and Moen C. D. (2014): Finite strip elastic buckling solutions for thin-walled metal columns with perforation patterns. Thin-Walled Structures, 79, 187-201.

[18] Pham C. H. (2017): Shear buckling of plates and thin-walled channel sections with holes. Journal of Constructional Steel Research, 128, 800-811.

[19] Moen C. D. and Schafer B. W. (2011): Direct strength method for design of cold-formed steel columns with holes. Journal of Structural Engineering, 137(5), 559-570.

[20] Moen C. D. and Schafer B. W. (2008): Experiments on cold-formed steel columns with holes. Thin-Walled Structures, 46(10), 1164-1182.

[21] Zhao J. Y., Sun K., Yu C. and Wang J. (2019): Tests and direct strength design on cold-formed steel channel beams with web holes. Engineering Structures, 184, 434-446.

[22] Wang L. P. and Young B. (2015): Beam tests of cold-formed steel built-up sections with web perforations. Journal of Constructional Steel Research, 115, 18-33.

[23] Wang L. P. and Young B. (2017): Design of cold-formed steel built-up sections with web perforations subjected to bending. Thin-Walled Structures, 120, 458-469.

[24] Li L. Y. (2004): Lateral-torsional buckling of cold-formed zed-purlins partial-laterally restrained by metal sheeting. Thin-Walled Structures, 42(7), 995-1011.

[25] Chu X. T., Ye Z. M., Kettle R. and Li L. Y. (2005): Buckling behaviour of cold-formed channel sections under uniformly distributed loads. Thin-walled Structures, 43, 531-542.

[26] Chu X. T., Ye Z. M., Li L. Y. and Kettle R. (2006): Local and distortional buckling of cold-formed zed-section beams under uniformly distributed transverse loads. International Journal of Mechanic Sciences, 48, 378-388.

[27] Chen J. K. and Li L. Y. (2010): Distortional buckling of cold-formed steel sections subjected to uniformly distributed transverse loading. International Journal of Structural Stability and Dynamics, 10 (5), 1017-1030.

[28] Schafer B.W. and Adany S. (2006). “Buckling analysis of cold-formed steel members using CUFSM: conventional and constrained finite strip methods.” In: 18th International Specialty Conference on Cold-Formed Steel Structures, Orlando, Florida, October.

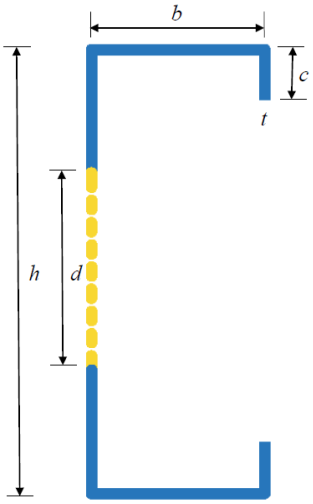

(a) Cross section

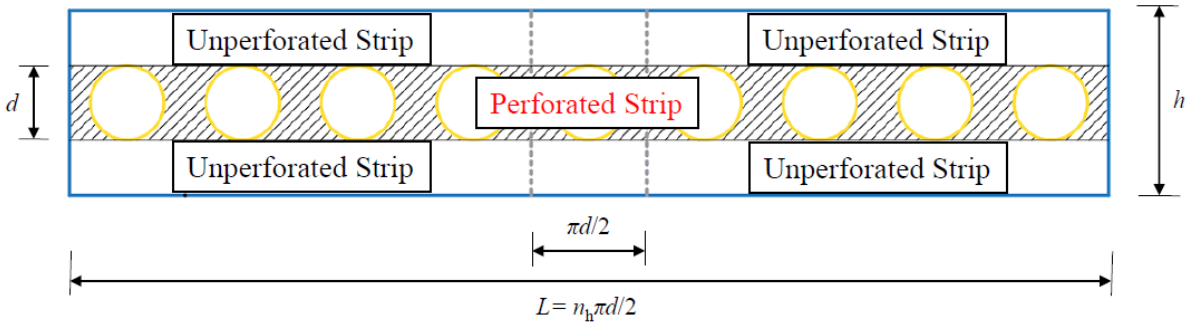

(b) Longitudinal direction

Fig.1 Notation and geometry used for PCFS beams (dimensions are defined based on the middle line of the section).

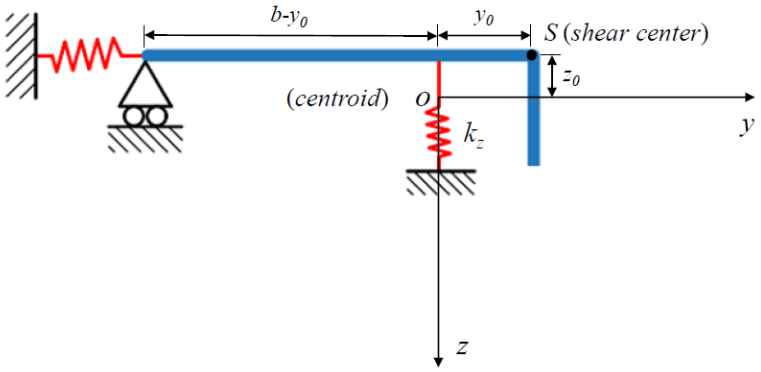

Fig.2 Analytical model proposed by Li and Chen [5].

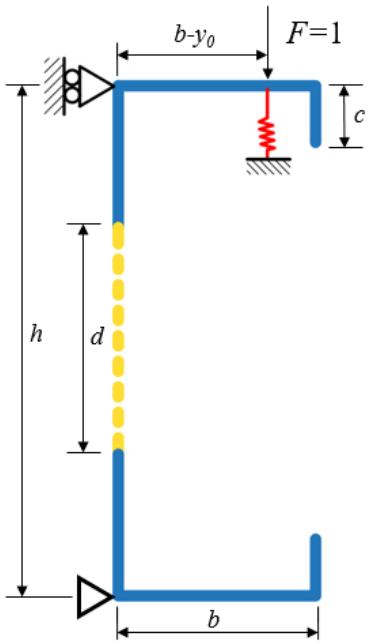

405

406 Fig.3 Model used for determining the stiffness of the vertical spring of the PCFS beam.

407

408

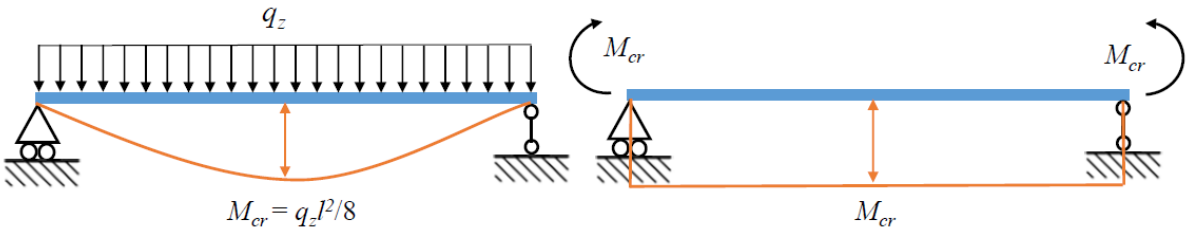

409

410 Fig.4 Bending moment diagram for uniformly distributed transverse loads (left) and pure
411 bending (right).

412

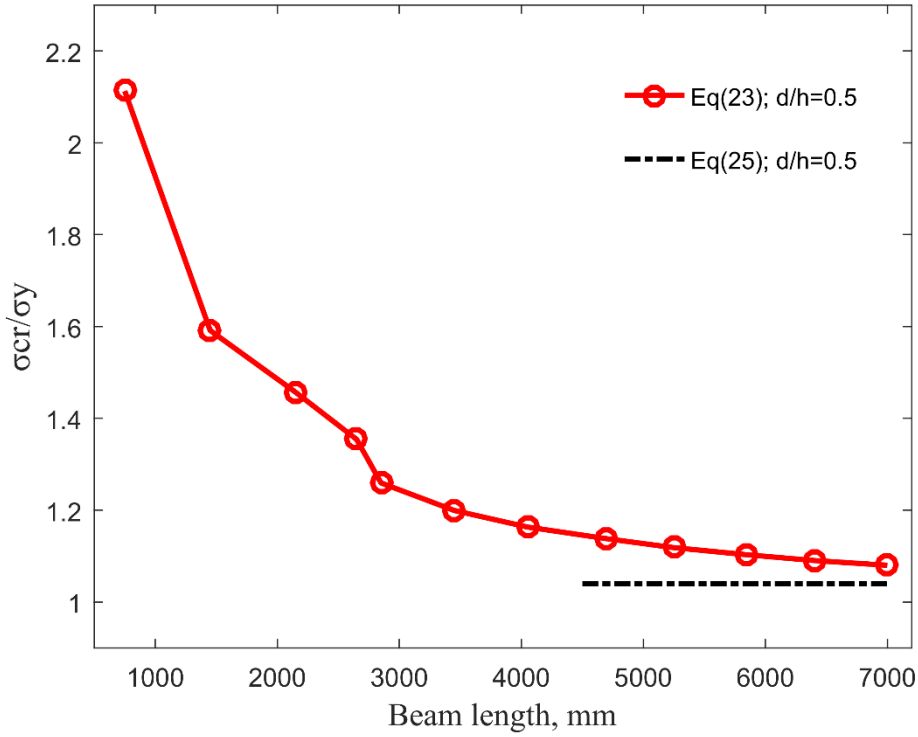

413

414 Fig.5 Comparison of the critical stress of PCFS beams between uniformly distributed
415 transverse loads (continuous line) and pure bending (dashed line) (h=200 mm, b=65 mm,
416 c=20 mm, t=2 mm, d=100 mm, σ_y=450 MPa).

417

418

419

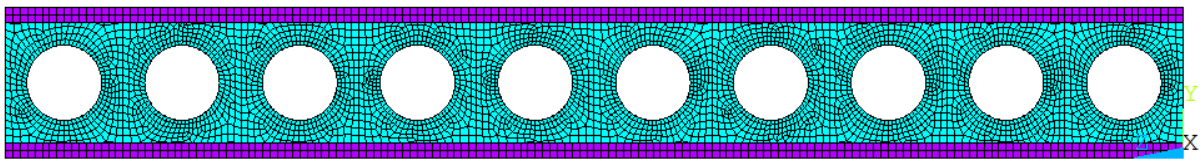

420

421 Fig.6 Typical finite element mesh of the PCFS beam (h=200 mm, b=65 mm, c=20 mm, t=2.5
422 mm, d=100 mm).

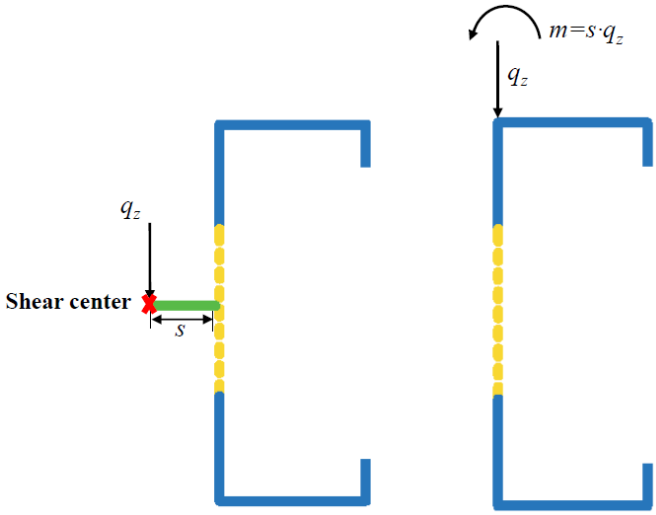

(a) (b)

Fig.7 Loading conditions of PCFS beams.

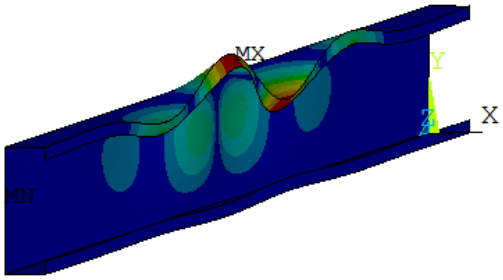

(a) d/h=0; *l*=3900 mm

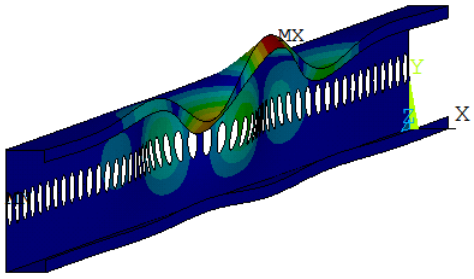

(b) d/h=0.25; *l*=4028 mm

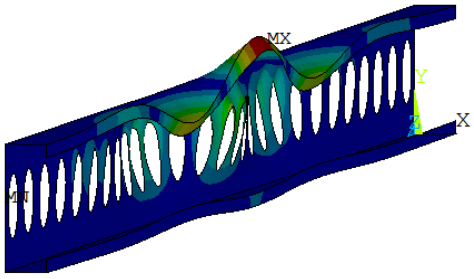

(c) d/h=0.5; *l*=4239 mm

Fig.8 Typical distortional buckling mode shapes of PCFS beams.

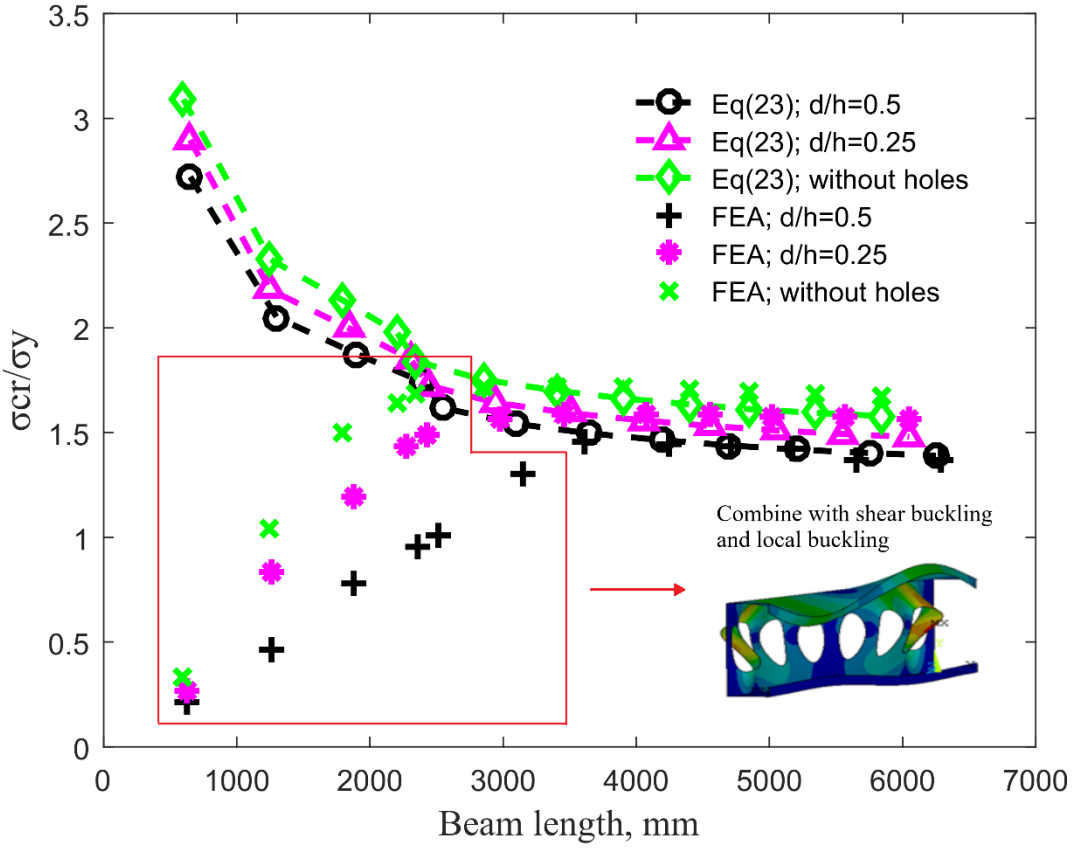

Fig.9 Comparison between analytical model and FEA of PCFS beams subjected to uniformly distributed transverse loads.

451 Table 1 Distortional half-wave lengths of CFS channel-sections from Albion Section

Section	Web depth (mm)	Flange width (mm)	Lip length (mm)	Thickness (mm)	Half-wave length (mm)
C12515	120	50	15	1.5	450
C12516	120	50	15	1.6	450
C14614	145	62.5	20	1.4	700
C14515	145	62.5	20	1.5	650
C14616	145	62.5	20	1.6	650
C14618	145	62.5	20	1.8	600
C14620	145	62.5	20	2	550
C17616	175	62.5	20	1.6	650
C17618	175	62.5	20	1.8	600
C17620	175	62.5	20	2	600
C17623	175	62.5	20	2.3	550
C17625	175	62.5	20	2.5	500
C20168	200	65	20	1.8	650
C20620	200	65	20	2	600
C20623	200	65	20	2.3	550
C20625	200	65	20	2.5	550
C22620	225	65	20	2	600
C22623	225	65	20	2.3	600
C22625	225	65	20	2.5	550
C24623	240	65	20	2.3	600
C24625	240	65	20	2.5	550
C24630	240	65	20	3	500
C26625	265	65	20	2.5	550
C26630	265	65	20	3	500
C30725	300	75	20	2.5	650
C30730	300	75	20	3	600

452